STUDY OF TRANSIENT CONDENSATION OCCURRING DURING THE STARTING OF THE EVAPORATION OF A DROPLET DEPOSITED ON A HEATED SUBSTRATE

by

Dorra KHILIFI[a,d*], Walid FOUDHIL[a,c], Kamel FAHEM[a], Souad HARMAND[b], and Sadok BEN JABRALLAH[a,c]

[a] Laboratory of Energetics and Thermal and Mass Transfer (LETTM), Science Faculty of Tunis, University of Tunis El Manar, Tunis, Tunisia
[b] University Polytechnique Hauts-de-France, LAMIH, UMR CNRS - 8201, F-59313 Valenciennes, France
[c] Science Faculty of Bizerte, University of Carthage, Bizerte, Tunisia
[d] Science Faculty of Tunis, University of Tunis El Manar, Tunis, Tunisia

Original scientific paper
https://doi.org/10.2298/TSCI181122377K

The evaporation of a drop deposited on a heated substrate is a complex process, which combines several phenomena such as the Marangoni effect, mass and thermal transfers, etc. We developed, in this paper, a mathematical model and a numerical simulation code used to carry out an in-depth study about the evaporation of a drop deposited on a heated substrate surrounded by air. This numerical study was supported by experimental work. The numerical findings obtained showed the existence of a condensation phenomenon for certain configurations. At the beginning of the experiment, the evaporation started at the triple point. However, a local region of the interface remained relatively cold. In this region, the concentration gradient (C_v, C_{sat}) directed from the liquid-gas interface to the air resulted in condensation of water steam. Although this phenomenon is temporary and visible only at the start of evaporation process, its study makes it possible to better understand and optimize the evaporation kinetics.

Key words: *sessile droplet, evaporation, steam diffusion, condensation*

Introduction

Evaporation of a droplet is used in various applications, such as spray drying, DNA mapping [1], combustion engineering [2, 3], cooling system [4], *etc*. The modelling of sessile droplet evaporation can be carried out by applying various approaches. In fact, several authors considered only the mass and heat transfers and the flow in the droplets. Other works improved the model by taking into account the diffusion in the air around the droplet, tab. 1.

In fact, the flow evaporated at the liquid-gas interface has been the subject of several works. For example, Khilifi *et al.* [5] studied experimentally the neighbourhood effect on the evaporation of a water drop. By carrying this study, they proved that the total evaporation of drops, which were close to each other, was noticeable minimized, compared to that of a single drop. This reduction was mainly due to the increase of the humidity in the vicinity of the liquid-gas interface of the drops.

* Corresponding author, e-mail: khelifidorrafst@gmail.com

Diddens *et al.* [6] studied the case of a binary droplet (water + ethanol) and showed that the condensation could appear on the zones of the interface characterized by a weak liquid molar fraction. This will happen even in the case of a dry environment. This phenomenon was also mentioned by [7] in the case of falling film evaporation.

In this work, we developed a model that describes the evaporation of a droplet deposited on a substrate by considering the ambient air and its dynamic properties. Simulation results were compared with the results of experiments carried out under the same conditions, which allowed for calculation of the local flow at the liquid-gas interface. In some parts of the interface and under specific conditions, this flow took on negative values, which resulted in condensation at the liquid-gas interface. Particular attention is paid to this phenomenon and the factors behind its appearance.

Table 1 summarizes various models proposed in the literature and compares them with the model developed in this work.

Table 1. Approach of modelling evaporation of a sessile droplet

Ref.	Conduction (solid)	Conduction (liquid)	Convection (liquid)	Convection (gas)	Diffusion	Numerical approach	Numerical method
[8]	x	x				Numerical	Finite volume
[9]		x	x		x	Numerical	Finite element
[10]	x	x			x	Numerical	Finite element
[11]	x	x	x		x	Numerical	Finite volume
[12]	x	x		x	x	Numerical	Finite volume
[13]	x	x	x		x	Analytique	
[14]	x	x	x			Numerical	Finite volume
[15]	x	x			x	Numerical	Finite volume
[16]	x	x			x	Numerical	Finite element
[17]	x	x	x	x	x	Numerical	Finite element
Present travail	x	x	x	x	x	Numerical	Finite element

Mathematical model

Figure 1 shows the physical domain, consisting of a liquid drop deposited on a solid substrate of silicon with thickness (e = 0.2 mm) and thermal conductivity, k_s. The evaporation is conducted at heating temperature T_h = 80 °C, an ambient temperature T_0 = 22 °C, relative humidity H = 50% and initial contact angle $\theta_0 = 80°$. A liquid droplet of radius, R, is evaporated in a constant contact line mode characterized by a decrease in contact angle and the pinning of the contact line. During the evaporation, the liquid-gas interface moves down following the normal vector n for the drop surface.

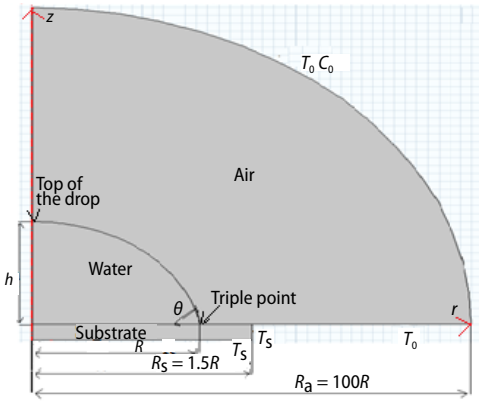

Figure 1. Descriptive sketch of a water droplet on heated silicon substrate

Initially, the drop has the shape of a half sphere because the surface tension, σ, dominates gravity and the contact radius R = 1.5 mm. Saturated vapor after the evaporation at the liquid-gas interface is transferred by diffusion into the moist air.

We admit that the problem is 2-D and symmetric. It is modelled in a cylindrical co-ordinates system (r, z).

The 2-D transport in the drop is made by convection and conduction. Outside of the drop, the heat and mass transfer are performed by conduction and diffusion, by taking into account the convection in the air, and for the substrate heat conduction is taken into consideration.

The ALE formulation

In this study, we adopt the ALE formulation (Arbitrary Lagrangian Eulerian Method) to model the movement of the gas-liquid interface. The ALE technique, based on the deformed mesh method, is an intermediate method between the Lagrangian method (the mesh following the movement of fluid particles) and the Eulerian method (fixing the mesh and associating a velocity droplet vector with each point). The ALE method combines the best components of the Lagrangian and Eulerian methods allowing to have mobile frontiers without moving the mesh. In this method, we introduce a third co-ordinate and PDE are formulated in the grid co-ordinate system. Thus, there are three co-ordinate systems, one related to space, x, another related to the domain, X, and the other is linked to the mesh, X_m. Therefore, the velocities are defined, $u(X, t)$ in the area and $u(X_\mathrm{m}, t)$ in the mesh [17]:

$$u\left(X,t\right)=\left(\frac{\partial X}{\partial t}\right)_X, \qquad u\left(X_\mathrm{m},t\right)=\left(\frac{\partial X}{\partial t}\right)_{X_\mathrm{m}} \tag{1}$$

A convective velocity is thus introduced:

$$u_\mathrm{c} = u(X, t) - u(X_\mathrm{m}, t) \tag{2}$$

In the conservation equations, $u(X_\mathrm{m}, t)$ is the flow velocity. In the advection term, the velocity is denoted as u_c [17]. In the rest, and to lighten the writing of the conservation equations, the velocity $u(X_\mathrm{m}, t)$ is denoted as u.

System of equations

The general equations describing the system are the Navier-Stokes (N-S) equations, continuity and energy in the liquid and gas phases also the conduction equation in the solid phase and the diffusion equation in the gas phase:

– Heat transfer equation in solid phase (substrate):

$$(\rho c_p)_\mathrm{s}\left(\frac{\partial T_\mathrm{s}}{\partial t}\right)=\nabla(k_\mathrm{s}\nabla T_\mathrm{s}) \tag{3}$$

– The N–S equations and continuity equation in liquid and gas phases:

$$\rho\left[\frac{\partial u}{\partial t}+\left(u_c\nabla\right)u\right]=\nabla\left\{-pI+\mu\left[\nabla u+\left(\nabla u\right)^T\right]\right\} \tag{4}$$

$$\nabla u = 0 \tag{5}$$

– Heat transfer equation in liquid and gas domain:

$$\rho c_p\left[\frac{\partial T}{\partial t}+\left(u_c\nabla\right)T\right]=\nabla\left[k\nabla T\right] \tag{6}$$

– Advection-diffusion equation in gas domain:

$$\frac{\partial c}{\partial t} + (u_c \nabla) C = \nabla (D \nabla C) \tag{7}$$

Initial conditions

At $t = 0$ seconds:

$$C = C_0 \quad \text{et} \quad T_g = T_0 = T_{amb} \quad \text{in gas domain} \tag{8}$$

$$T_l = T_0 \quad \text{in liquid domain} \tag{9}$$

$$T_s = 80\ °\text{C} \quad \text{in solid domain} \tag{10}$$

Boundary conditions

The boundary conditions are applied at three locations: liquid-solid interface, liquid-gas interface and axis of symmetry.

– At the liquid-solid interface :

$$u = 0 \tag{11}$$

$$0 \le r \le R \quad \text{at} \quad z = 0, \quad k_s \frac{\partial T}{\partial z} = k_l \frac{\partial T}{\partial z} \tag{12}$$

$$R < r < R_s \quad \text{at} \quad z = 0, \quad \frac{\partial C}{\partial z} = 0 \tag{13}$$

– At $z = -e$:

$$T_s = 80\,°\text{C} \tag{14}$$

– At $r = 0$ (axisymmetric conditions are applied):

$$un = 0 \tag{15}$$

$$\left\{ -pI + \mu \left[\nabla u + (\nabla u)^T \right] \right\} n = 0 \tag{16}$$

$$-n(-D \nabla C) = 0 \tag{17}$$

$$-n\left(-k \nabla T\right) = 0 \tag{18}$$

– At $r = R_a$:

$$T = T_0 \tag{19}$$

$$C = C_0 \tag{20}$$

Gas-liquid interface conditions

The balance of the constraints at the liquid-gas interface [17]:

$$n\boldsymbol{\tau}_g = n\boldsymbol{\tau}_l + f_{st} \tag{21}$$

where $\boldsymbol{\tau}_g$ and $\boldsymbol{\tau}_l$ are the total constraint tensors in the liquid and gas phases, respectively, at the liquid-gas interface, n – the normal at the interface, and f_{st} – the force per surface unit owing to the surface tension [17]:

$$f_{\mathrm{st}} = \sigma(\nabla_{\mathrm{s}} n)n - \nabla_{\mathrm{s}}\sigma \tag{22}$$

where ∇_{s} is the surface gradient operator:

$$\nabla_{\mathrm{s}} = (I - nn^{\mathrm{T}})\nabla \tag{23}$$

We can also represent the force, f_{st}, by two components, normal and tangential directions of the boundary. So, the force balance, in, respectively, normal and tangential directions, is given [17]:

$$(n\boldsymbol{\tau}_{\mathrm{g}} - n\boldsymbol{\tau}_{\mathrm{l}})n = \frac{\sigma}{r_c}n \tag{24}$$

$$(n\boldsymbol{\tau}_{\mathrm{g}} - n\boldsymbol{\tau}_{\mathrm{l}})\vec{\mathrm{t}} = -\sigma_{\mathrm{T}}\nabla_{\mathrm{s}}T \tag{25}$$

where r_{c} is the curvature radius, and $\vec{\mathrm{t}}$ is the tangential vector of the interface.

The right term in the previous equation is the thermocapillary constraint owing to the temperature difference at the interface, which causes the Marangoni effect, with [17]:

$$\sigma_{\mathrm{T}}(T) = \sigma_0 - \left|\frac{\mathrm{d}\sigma}{\mathrm{d}T}\right|(T - T_0)\,. \tag{26}$$

where σ_0 is the surface tension at the temperature T_0 of the environment.

The vapor is assumed to be saturated at the liquid-gas interface. An empirical relationship between T_{sat} and $P_{v,\mathrm{sat}}$ is employed to calculate the saturated vapor pressure at the interface (Rankine formula):

$$P_{v,\mathrm{sat}} = \mathrm{e}^{\left[13{,}7 - \frac{5120}{T_{\mathrm{sat}}}\right]} \cdot 10^5 \tag{27}$$

This, in turn, is converted into vapor concentration at the liquid-gas interface using the ideal gas law:

$$C_{\mathrm{sat}} = \frac{P_{v,\mathrm{sat}}}{\mathrm{R}T_{\mathrm{sat}}} \tag{28}$$

The local mass loss of the liquid (*i. e.*, local evaporation flux) is calculated from the vapor diffusion at the liquid-gas interface [17]:

$$m_{\mathrm{ev}} = n(-D\nabla C)M_r \tag{29}$$

where M_r is the molar mass of the liquid molecules. The mass balance at the liid-gas interface can be expressed [17]:

$$u_{\mathrm{g}} - u_{\mathrm{l}} = \left(\frac{1}{\rho_{\mathrm{g}}} - \frac{1}{\rho_{\mathrm{l}}}\right)(-m_{ev})n \tag{30}$$

The velocity of mesh u_{mesh}, which is used as a boundary condition for mesh movement at the liquid-gas interface can be calculated [17]:

$$u_{\mathrm{mesh}} = \left(u_{\mathrm{l}}n + \frac{m_{\mathrm{ev}}}{\rho_{\mathrm{l}}}\right)n \tag{31}$$

Although the temperature is continuous cross the liquid-gas interface, the thermal balance at the interface can be written in the following form [17]:

$$n\left[k_g\left(\nabla T\right)_g - k_l\left(\nabla T\right)_l\right] = -m_{ev}h_{fg} \tag{32}$$

Numerical procedure

The simulation of the problem was achieved by using the calculating code COMSOL Multiphysics Version 4.2b. This code offers the ability to track, the gas-liquid interface of the droplet over time when the liquid domain deforms and narrows following the process of evaporation.

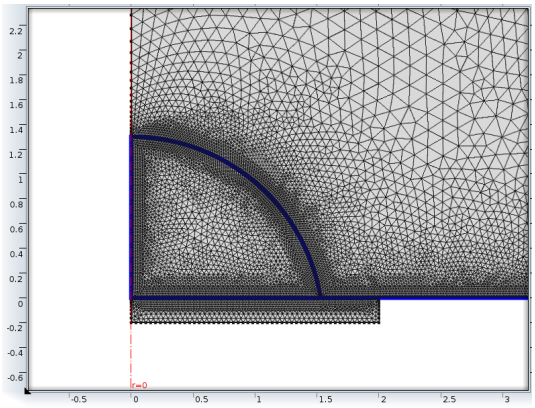

Figure 2. Typical mesh in the drop and its vicinity

Figure 2 shows the typical mesh adopted in this study. The mesh is narrowed mainly at the borders especially along the liquid interfaces. The numerical difficulty of the problem lies in having to simulating a physical problem characterized by a variable interface in time and space. The deformed mesh method is implemented with the Comsol code. It is convenient for cases where boundaries move as a function of time. The idea of the method is not to generate a new mesh for each border configuration, but just to disrupt nods mesh to adopt to the displaced mesh.

Results

Validation

In heir study Yang *et al.* [17], studied the variations in the relative difference of the average temperatures at the liquid-gas interface during specific times. They showed that a quasi-stationary regime is established after $\Delta t = 3$ seconds for an initial contact angle $\theta_0 = 90°$. The present model allowed this result under the following conditions: initial angle $\theta_0 = 90°$, ambient temperature $T_0 = T_h = 25$ °C and humidity $H = 38\%$. The curve in fig. 3 shows a comparison with this study and indicates good quantitative agreement.

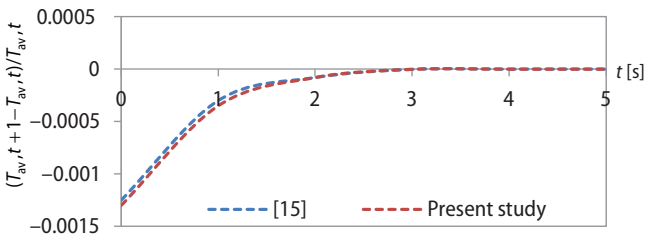

Figure 3. Numerical validation with Yang *et al.* [15]

Description of the phenomenon of condensation

We studied the evaporation of a droplet of liquid deposited on a heated substrate, fig. 4, that resulted from a mass flow at the interface generated by the concentration gradient. However, the direction of this flow depended on that of the mass gradient, according to Fick's law:

$$m_{ev} = -D\left(\frac{\partial C}{\partial n}\right) \tag{33}$$

If the concentration of water steam in the air around the immediate vicinity of the liquid-gas interface was greater than that at the liquid-gas interface, according to eq. (33), a motion of water steam particles towards the liquid-gas interface is observed. This phenomenon clearly observed in our study is called condensation.

The curves presented in figs. 4(a) and 4(b) show the temperature and concentratn variations, respectively, at the liquid-gas interface for different times at a heating temperature $T_h = 80$ °C.

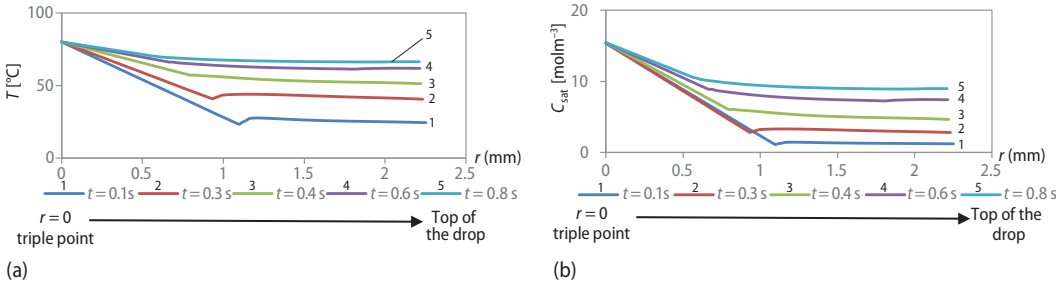

Figure 4. Temperature (a) and concentration (b) variations at liquid-gas interface (from triple point to top of drop) for different times: $T_h = 80$ °C, $T_0 = 22$ °C, $H = 50\%$ and $\theta_0 = 80°$

These curves demonstrate two phenomena:

– A first area is located between the triple point and a point at the liquid-gas interface that varies with the time. It is characterized by a decrease in the temperature and concentration curves.
– A second region representing the transition area is characterized by relatively constant values of temperature and concentration.

At the beginning of heating (curves relative to the instants 0.1 and 0.3 seconds), we observe that temperature decreases rapidly from the triple point to a transition zone from which the temperature becomes more or less constant to the top of the drop.

As a function of the progress of the heating time (from 0.8 seconds), and after the phenomena of diffusion and convection in the droplet, we notice a partial thermal homogenization at the interface of the droplet. Therefore, the slope of the temperature from the triple point becomes less important, and the transition zone moves toward the triple point. These phenomena are almost similar on the curves of the evolution saturation concentration, fig. 5(b), at the interface.

Figure 5 demonstrates the temporal variation of the evaporated local flux at the liquid-vapor interface. The represented curves show the negative values of the evaporated local flux ($m_{ev} < 0$), which proves the appearance of condensation on an area of the liquid-vapor interface. This same result was obtained also by Diddens *et al.* [6] in the case of binary droplets (water + ethanol).

Besides, from fig. 5, we conclude that, depending on the progress of the heating time, the area of condensation moves towards the triple point of the drop and this phenomenon becomes more and more negligible.

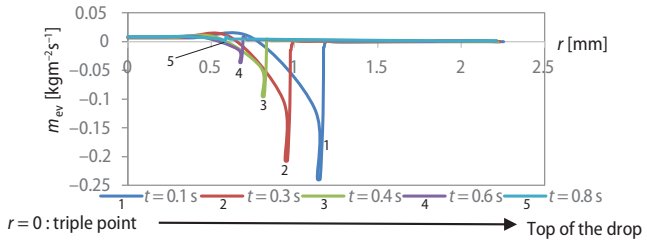

Figure 5. Temporal variations in local flow evaporated at liquid-gas interface (from triple point to top of drop) for different times: $T_h = 80$ °C, $T_0 = 22$ °C, $H = 50\%$ and $\theta_0 = 80°$

To explain the appearance of condensation at the beginning of our experiments, we represent the variations of temperature and concentration as a function of time, figs. 6(c) and 6(d): in an area of the liquid-gas interface, which presents the condensation zone and in the air around the immediate vicinity of the condensation zone.

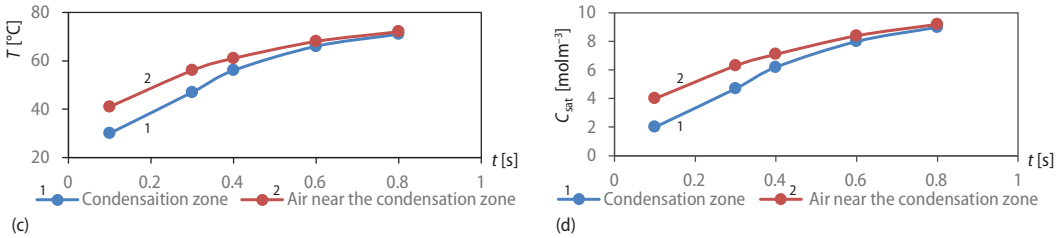

Figure 6. Temperature (c) and concentration (d) variations as function of time: $T_h = 80$ °C, $T_0 = 22$ °C, $H = 50\%$ and $\theta_0 = 80°$

These figures show that, at the start of evaporation ($t = 0.1$ and $t = 0.3$ seconds), the temperature and concentration in the air around the condensation zone are greater than those in the condensation zone, which produces temperature gradient (T_v, T_{sat}) and concentration gradient (C_v, C_{sat}) towards humid air. Obviously, temperature and concentration gradients decrease over time until they become negligible at $t = 0.8$ seconds. the air carried on by the flow.

Indeed, at the beginning of the experiment, the evaporation started at the triple point, while a local region of the liquid-gas interface remained relatively cold. The vicinity is characterized by humid air carried on by the flow, as shown in fig. 7. We note that the temperature and concentration of this humid air were higher than those of a region of liquid-gas interface. Thus, a concentration gradient, directed from the liquid-gas interface to the air, was observed in this region. The concentration gradient resulted in an evaporation flux in the opposite direction in accordance with Fick's law, eq. (33), this phenomenon, called condensation, disappeared at $t = 0.8$ seconds, as shown in fig. 5, and was limited in time.

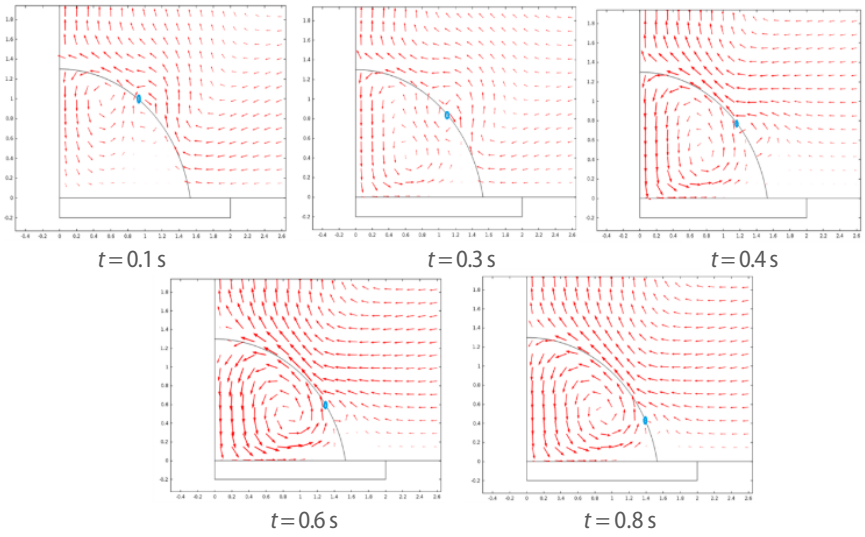

Figure 7. Velocity fields in liquid and gaseous phases for five configurations (blue spot is maximum position of condensation) (*for color image see journal web site*)

Indeed, the attenuation of condensation as a function of time could be due to the internal convective circulation of water in the drop, fig. 7, which, together with thermal diffusion, accelerated both temperature homogenization at liquid-gas interface and consequently as well as the attenuation of both temperature gradient (T_v, T_{sat}) and concentration gradient (C_v, C_{sat}): condensation engine.

It is worth-noting that these zones of condensation correspond to the transition points of the curves representing the variation of the temperature and the concentration at liquid-gas interface, fig. 4. The transition point *c* is the point closest to the triple point and is characterized by a low temperature value and therefore a low saturation concentration value. This condition favours the condensation in point *c*. Indeed, the transition point, denoted by *c*, corresponds to the condensation maximum point.

Figure 8 depicts the evolution of the position of the maximum condensation point at the liquid-gas interface. It is possible to follow the displacement of the condensation zone by the displacement of the max condensation point *c* at the interface liquid-gas. In fact, the movement of the condensation zone towards the triple point over time can be explained by the localized heating of the surface on which the condensation occurs. Thus, the condensation must extend to more adequate area from the viewpoint of proximity and temperature deviation from the hottest triple point.

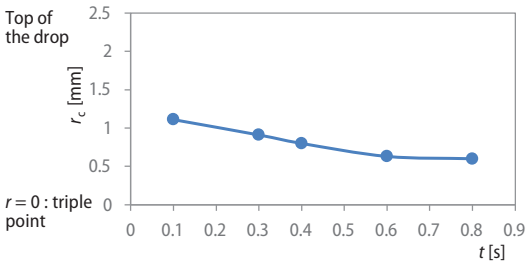

Figure 8. Evolution the position of maximum condensation point *c* at interface liquid-gas (from triple point to top of drop) as function of time: T_h = 80 °C, T_0 = 22 °C, H = 50% and θ_0 = 80 °

Experimental study

We are interested, in this section, in investigating experimentally the evaporation of the water drop deposited on a heated substrate and more specifically in examining the existence of condensation phenomenon. Considering the experimental difficulty of measuring the condensation local flow, we describe condensation by showing, at the beginning of the experiment, the appearance of a significant temperature gradient at the liquid-gas interface, which is the engine of condensation.

Experimental set-up

The glass substrate was placed in a vapor chamber (14 × 12.4 × 7.5 cm^3) in which the ambient temperature and relative humidity could be controlled and set to 22 °C and 40%, respectively, fig. 9. A droplet of water of volume 0.9 µl was deposited on a heated glass substrate (T_h = 70 °C) by means of a programmable syringe (KD Scientific Legato 100), resulting in a deposit radius *R* of about 0.9 mm.

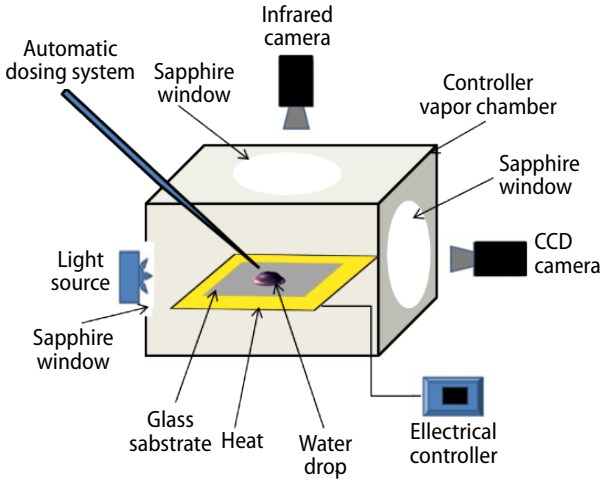

Figure 9. Schema of the experimental set-up

The air inside of the chamber is at rest. The top of the vapor chamber has a sapphire window for the infrared camera and a hole for passing the syringe. An infrared camera (FLIR X6580SC, 640 × 512 pixels, 15 μm detector pitch) is installed on the top for infrared thermal mapping and visualization of thermal instabilities on the surface of the droplets.

A Kruss Drop Shape Analyzer is used to measure the contact angle, volume, diameter, and height of the sessile droplets during evaporation. A side-view CCD camera (Allie Vision Technologies, 780 × 580 pixels) records the evaporation process of the droplets for profile analysis.

Experimental results

In this section, we study the thermal behaviour of the droplet at the beginning of the evaporation. The objective of this study consists in representing the important temperature gradient at the liquid-gas interface just at the start of evaporation process (in the first milliseconds).

Figure 10 illustrates the variation of the temperature at the liquid-gas interface for different times at a heating temperature T_h = 70 °C.

Figure 11 demonstrates the evolution of the temperature difference (ΔT) over time at the liquid-gas interface between the triple point and the transition point *c* at which the temperature becomes more or less constant to the top of drop.

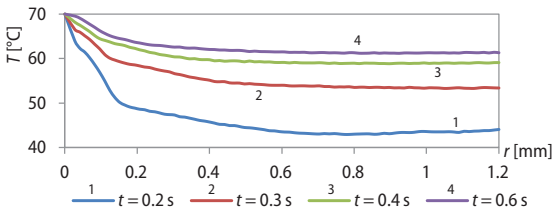

Figure 10. Variations in temperature at liquid-gas interface (from triple point to top of drop) of different times: T_h = 70 °C, T_0 = 22 °C, H = 40% and θ_0 = 65°

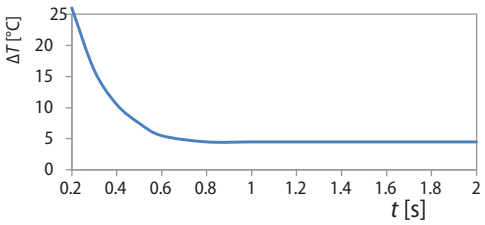

Figure 11. Evolution of temperature difference at liquid-gas interface *vs.* time: T_h = 70 °C, T_0 = 22 °C, H = 40% and θ_0 = 65°

At the start of the heating process (curves at times 0.2 and 0.3 seconds), a large temperature difference was observed at the liquid-gas interface from the triple point to a transition point *c*. As a function of the progress of the heating time, the slope of the temperature from the triple point became considerably less important, which reflects the evolution of the saturation concentration along the interface.

In addition, from figs. 10 and 12, we notice that, depending on the progress of the heating time, the transition point *c* of the curves representing the variation of the temperature at liquid-gas interface moves towards the triple point of the drop, which was proved in the simulation part. The transition point *c* is the point closest to the triple point and is characterized by a low temperature value and therefore a low saturation concentration value. This condition favours the condensation in point *c*. Indeed, the transition point, denoted by *c*, corresponds to the condensation maximum point.

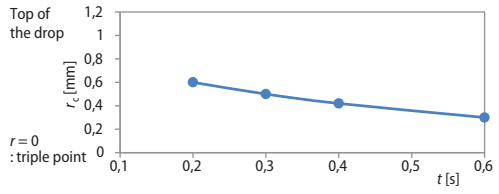

Figure 12. Evolution of the position of the transition point *c* at interface liquid-gas (from triple point to top of drop) as function of time: T_h = 70 °C, T_0 = 22 °C, H = 40% and θ_0 = 65°

Figure 13 represents the process of water drop evaporation over time. At the beginning of this process, fig. 13(f), the images of instants

0.2, 0.3, and 0.6 seconds show a very important temperature gradient at the liquid-gas interface. In these first milliseconds, we clearly observe the internal convective circulation of water in the drop (Marangoni intense temperature). The direction of the movement is represented by arrows on the images of 0.2 seconds. This temperature difference, especially through its effect on mass gradient, can be considered as the main factor of condensation phenomenon, which was explained in the simulation part.

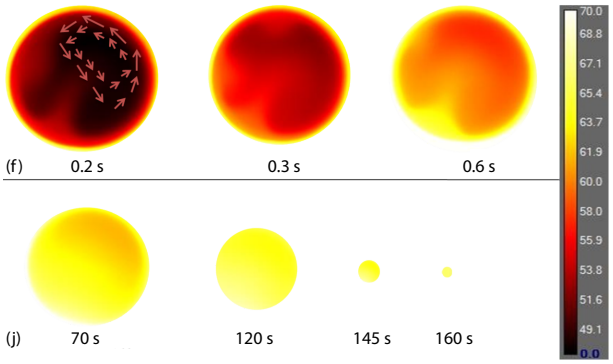

Figure 13. Snapshots from infrared video camera of evaporation process of water drop (f) in first milliseconds and (j) until total disappearance

Figure 13(j) describes the evaporation process until the drop total disappearance. We notice a partial thermal homogenization on the drop liquid-gas interface and consequently the condensation total disappearance. This figure confirms the results previously presented in figs 10 and 11.

In this part, the experimental results are compared with the numerical ones; for an initial contact angle of 65° (glass substrate), heating temperature T_h = 70 °C, ambient temperature T_0 = 22 °C, relative humidity H = 40% and diameter of the radius R = 0.9 mm.

Figure 14 shows a comparison between the results of the simulations and those of the experiments; for the variation in temperature difference, ΔT, over time at liquid-gas interface between the triple point and the transition point c. The difference in temperature is more important during the interval of time [0-0.6 seconds]. Then, it remains constant. This is the interval of time where condensation occurs.

A second comparison is proposed in fig. 15, where we present the variation ov time of the position of the transition point c, at the liquid-gas interface. Depending on the progress of the heating time, the transition point c moves towards the triple point of the drop.

Figures 14 and 15 reveal a satisfactory agreement between the results of the simulation and the experimental finding.

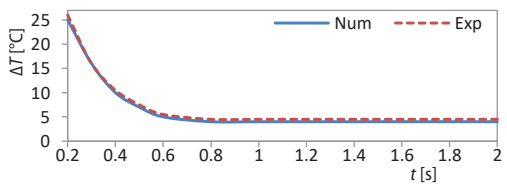

Figure 14. Evolution of temperature difference at liquid-gas interface *vs.* time: T_h = 70 °C, T_0 = 22 °C, H = 40% and θ_0 = 65°

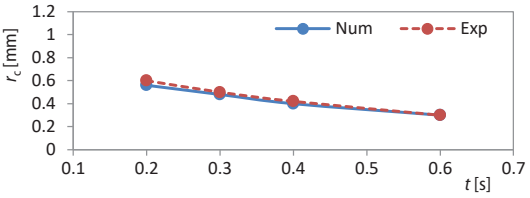

Figure 15. Evolution of the position of the transition point c at interface liquid-gas (from triple point to top of drop) as function of time: T_h = 70 °C, T_0 = 22 °C, H = 40% and θ_0 = 65°

Conclusion

In this work, we describe numerically and experimentally the phenomenon of condensation in the beginning of evaporation (< 1 second) of a droplet deposited on a heated substrate.

The condensation is a transient and short-lived phenomenon that appears at the early stage of evaporation of the droplet. This phenomenon resulted from:

- The appearance of a significant temperature gradient throughout the liquid-gas interface just at the beginning of the experiments.
- The movement of water vapor produced at the triple point (meaning Marangoni).

Moreover, we revealed that the condensation area decreases and becomes closer to the triple point as a function of time.

The obtained results helped to better understand the kinetics of droplet evaporation. In addition, in some industrial applications, condensation is perceived as delaying evaporation. Thus, a more adequate distribution of the heating between the droplet and the substrate to reduce energy consumption needed during the evaporation process.

Nomenclatures

C – molar concentration, [molm^{-3}]
D – diffusion coefficient, [m^{2}s^{-1}]
e – thickness, [mm]
H – relative humidity
k – thermal conductivity, [Wm^{-1}K^{-1}]
m_{ev} – local evaporation flow, [kgm^{-2}s^{-1}]
M_r – molar mass, [kgmol^{-1}]
n – normal vector
p – pressure, [Pa]
r, z – cylindrical co-ordinates, [mm]
R – droplet radius, [mm]
R – universal gas constant, [Jmol^{-1}K^{-1}]
$\vec{t}$ – tangential vector
T – temperature, [K]
t – time, [s]
u – velocity, [ms^{-1}]

Greek symbols

θ – contact angle, [°]
μ – dynamic viscosity, [Pas]
ρ – density, [kgm^{-3}]
σ_T – temperature coefficient of surface tension, [Nm^{-1}K^{-1}]
σ – surface tension, [Nm^{-1}]
$\boldsymbol{\tau}$ – stress tensor, [Nm^{-2}]

Subscripts

0 – environmental condition
av – average
condt – conduction
cond – condensed
conv – convection
g, l, s – gas, liquid, solid phase
sat – saturated
s – substrate
v – water steam

References

[1] Wang, W., *et al.*, Scanning Force Microscopy of DNA Molecules Elongated by Convective Fluid Flow in an Evaporating Droplet, *Biophysical Journal*, *75* (1998), 1, pp. 513-520
[2] Saito, M., *et al.*, Evaporation and Combustion of a Single Fuel Droplet in Acoustic Fields, *Fuel*, *73* (1994), 3, pp. 349-353
[3] Murko, V. I., *et al.*, Investigation of the Spraying Mechanism and Combustion of the Suspended Coal Fuel, *J. Thermal Science, 19* (2015), 1, pp. 243-251
[4] Chen, Z., *et al.* Numerical Simulation of Single-Nozzle Large Scale Spray Cooling on Drum Wall, *J. Thermal Science, 22* (2018), 1A, pp. 359-370
[5] Khilifi, D., *et al.,* Study of the Phenomenon of the Interaction between Sessile Drops During Evaporation, *Thermal Science*, *23* (2019), 2B, pp. 1105-1114
[6] Diddens, C., *et al.*, Modeling the Evaporation of Sessile Multi-Component Droplets, *Journal of Colloid and Interface Science*, *487* (2017), Feb., pp. 426-436
[7] Ben Jabrallah, S., Convective Heat and Mass Transfer with Evaporation of a Falling Film in a Cavity. *International Journal of Thermal Sciences, 45* (2006), 1, pp. 16-28
[8] Chandra, S., *et al.*, Effect of Liquid-Solid Contact Angle on Droplet Evaporation, *Fire Safety Journal, 27* (1996), 2, pp. 141-158
[9] Mollaret, R., *et al.*, Experimental and Numerical Investigation of the Evaporation into Air of a Drop on a Heated Surface, *Chem. Eng. Res. Des*., *82* (2004), 4, pp. 471-480

[10] Widjaja, E., Harris, M. T., Numerical Study of Vapor Phase Diffusion Driven Sessile Drop Evaporation, *Computers and Chemical Engineering, 32* (2008), 10, pp. 2169-2178
[11] Strotos, G., *et al.*, Numerical Investigation on the Evaporation of Droplets Depositing on Heated Surfaces at Low Weber Numbers, *International Journal of Heat and Mass Transfer, 51* (2008), 7-8, pp. 1516-1529
[12] Ait Saada, M. *et al.*, Evaporation of a sessile drop with pinned or receding contact line on a substrate with different thermophysical properties*, International journal of heat and mass transfer,* 58 (2013), 1-2, pp. 197-208
[13] Semenov, S., *et al.*, Evaporation of Sessile Water Droplets: Universal Behaviour in Presence of Contact Angle Hysteresis, *Colloids and Surfaces A: Physicochem. Eng. Aspects, 391* (2011), 1-3, pp. 135-144
[14] Lu, G., Internal Flow in Evaporating Droplet on Heated Solid Surface, *International Journal of Heat and Mass Transfer, 54* (2011), 19-20, pp. 4437-4447
[15] Ait Saada, M., Numerical Investigation of Heated an Mass Transfer of an Evaporating Sessile Drop on a Horizontal Surface, *Phys.Fluid, 22* (2010), 11, pp. 112-115
[16] Lopes, M. C., *et al.*, Influence of the Substrate Thermal Properties on Sessile Droplet Evaporation: Effect of Transient Heat Transport, *Colloids and Srfaces A: Physiocochem. Eng. Aspects, 432* (2013), Sept., pp. 64-70
[17] Yang, K., *et al.*, A Fully Coupled Numerical Simulation of Sessile Droplet Evaporation Using Arbitrary Lagrangian-Eulerian Formulation, *International Journal Heat and Mass Transfer, 70* (2014), 11, Mar., pp. 409-420

Paper submitted: November 22, 2018
Paper revised: August 29, 2019
Paper accepted: September 6, 2019

© 2020 Society of Thermal Engineers of Serbia
Published by the Vinča Institute of Nuclear Sciences, Belgrade, Serbia.
This is an open access article distributed under the CC BY-NC-ND 4.0 terms and conditions